Isotropic-nematic interfacial tension of hard and soft rods: Application of advanced grand canonical biased-sampling techniques

R. L. Vink, S. Wolfsheimer, and T. Schilling

Citation: J. Chem. Phys. **123**, 074901 (2005); doi: 10.1063/1.2000237
View online: http://dx.doi.org/10.1063/1.2000237
View Table of Contents: http://jcp.aip.org/resource/1/JCPSA6/v123/i7
Published by the AIP Publishing LLC.

Isotropic-nematic interfacial tension of hard and soft rods: Application of advanced grand canonical biased-sampling techniques

R. L. C. Vink,[a] S. Wolfsheimer, and T. Schilling
Institut für Physik, Johannes Gutenberg Universität, D-55099 Mainz, Staudinger Weg 7, Germany

(Received 15 June 2005; accepted 21 June 2005; published online 19 August 2005)

Coexistence between the isotropic and the nematic phase in suspensions of rods is studied using grand canonical Monte Carlo simulations with a bias on the nematic order parameter. The biasing scheme makes it possible to estimate the interfacial tension γ_{IN} in systems of hard and soft rods. For hard rods with $L/D=15$, we obtain $\gamma_{IN}\approx 1.4k_BT/L^2$, with L the rod length, D the rod diameter, T the temperature, and k_B the Boltzmann constant. This estimate is in good agreement with theoretical predictions, and the order of magnitude is consistent with experiments. © *2005 American Institute of Physics*. [DOI: 10.1063/1.2000237]

I. INTRODUCTION

The aim of this paper is to present a computation of the interfacial tension γ_{IN} between the coexisting isotropic and nematic (IN) phase in suspensions of monodisperse hard rods via computer simulation. While the hard-rod fluid simplifies experimental reality, ignoring, for example, long-ranged interactions and polydispersity,[1] it nevertheless captures the main mechanism of the IN phase transition and serves as a valuable model system. Experiments have shown that γ_{IN} is very small, typically in the range of $10^{-3}-10^{-4}$ mN/m,[1] which makes it difficult to extract γ_{IN} from simulation data. Simulation estimates of γ_{IN} are therefore rare, and have only been reported for ellipsoids,[2,3] soft rods,[4] and lattice models.[5] Theoretical estimates are more abundant,[6–11] but are usually obtained in the Onsager limit[12] of infinite rod length ($L/D\to\infty$). The case of finite rod length is more difficult to describe theoretically, but has been addressed in Ref. 9 using density-functional theory and in Ref. 8 using a scaling relation. At the time of writing, no simulation estimate of γ_{IN} for the hard-rod fluid has been reported. Such an estimate would clearly be valuable to test theoretical predictions and to see if the order of magnitude of γ_{IN} observed in experiments is reproduced.

Despite its simplicity, simulating the hard-rod fluid is not trivial.[13,14] The bottleneck is the hard-particle interaction, which complicates both molecular-dynamics (MD) and Monte Carlo (MC) methods. In the case of MD, the discontinuous potential prevents the calculation of smooth forces. In the case of MC, equilibration times are long due to very low acceptance rates. An important improvement is the use of soft interactions, as was done for ellipsoids[2,3] and rods.[4,15] By using soft interactions, the qualitative phase behavior is usually retained, but simulations become much more efficient. Moreover, MC simulations in the grand canonical ensemble become possible, enabling the investigation of IN coexistence via the probability distribution in the particle number density. This technique is well established in simulations of fluid-vapor coexistence,[16–20] and was recently extended to IN coexistence in suspensions of soft rods.[4] The advantage of grand canonical simulations is that the coexistence densities, as well as the interfacial tension, can be obtained.

Since coexisting phases are separated by a free-energy barrier arising from the interfacial tension,[21] it is essential to use a biased sampling scheme to access regions of high free energy. In simulations of fluid-vapor coexistence, the bias is usually put on the density. While a density bias has also been used to simulate IN coexistence,[4] this choice is not optimal. In simulations that rely on standard MC moves, such as random translations and rotations of single particles, it is difficult to reach the nematic phase starting from the isotropic phase simply by increasing the density because the orientational degrees of freedom relax only very slowly.[22] This effect is called "jamming," and it explains why the simulations of Ref. 4 were limited to rather small systems.

In this work, grand canonical MC simulations using a bias on the nematic order parameter are performed. As we will show, this approach is much less susceptible to jamming, and enables simulations of large systems. This in turn allows for accurate estimates of the interfacial tension in suspensions of soft rods. As an additional bonus, a bias on the nematic order parameter paves the way towards grand canonical simulations of hard rods, enabling a simulation estimate of γ_{IN} for the hard-rod fluid.

The outline of this paper is as follows: First, we introduce the liquid-crystal model used in this work. The biased sampling scheme is described next. The results are presented in Sec. IV. We end with a summary and a comparison to theoretical predictions in the last section.

II. MODEL AND ORDER PARAMETERS

We consider rods of elongation L and diameter D. The simulations are performed in a three-dimensional box of size $L_x\times L_y\times L_z$ using periodic boundary conditions in all dimensions. In this work, we fix $L_x=L_y$, but we allow for elongation in the remaining dimension $L_z\geqslant L_x$. Moreover, to avoid double interactions between rods through the periodic

[a]Electronic mail: vink@uni-mainz.de

boundaries, we set $L_x > 2L$. The position of the center of mass of rod i is denoted $\mathbf{r}_i$, and its orientation $\mathbf{u}_i$, with normalization $|\mathbf{u}_i| = 1$. The interaction between two rods i and j is given by a pair potential of the form

$$v_{ij}(r) = \begin{cases} \epsilon, & r < D, \\ 0, & \text{otherwise}, \end{cases} \tag{1}$$

with r the distance between two line segments of length L, see also Ref. 4. The total energy is thus a function of the center-of-mass coordinates and the orientations of all rods

$$E(\mathbf{r}_1, \ldots, \mathbf{r}_N; \mathbf{u}_1, \ldots, \mathbf{u}_N) = \sum_{i=1}^{N} \sum_{j=i+1}^{N} v_{ij}, \tag{2}$$

with N the number of rods in the system (in the following we will drop the $\mathbf{r}_i$ and $\mathbf{u}_i$ dependences in our notation).

To investigate the IN transition, the density and the average rod alignment are used as order parameters. Since the density in the isotropic phase is lower than in the nematic phase, the rod number density $\rho = N/V$ may be used to distinguish the phases, with V the volume of the simulation box. Following convention, we also introduce the reduced density $\rho^\star = \rho/\rho_{\mathrm{cp}}$, with $\rho_{\mathrm{cp}} = 2/[\sqrt{2} + (L/D)\sqrt{3}]$ the density of regular close packing of hard rods.[13]

In the nematic phase the rods are, on average, aligned, whereas in the isotropic phase the rods are randomly oriented. Therefore, the nematic order parameter may also be used to distinguish the phases. The latter quantity is defined in terms of the orientational tensor Q, whose components are given by

$$Q_{\alpha\beta} = \frac{1}{2N} \sum_{i=1}^{N} (3u_{i\alpha}u_{i\beta} - \delta_{\alpha\beta}), \tag{3}$$

with $u_{i\alpha}$ the α component ($\alpha = x, y, z$) of the orientation of rod i and $\delta_{\alpha\beta}$ the Kronecker delta. In this work, the maximum eigenvalue S of the orientational tensor is taken as the nematic order parameter, being close to unity in the nematic phase and close to zero in the isotropic phase. The eigenvector corresponding to S is called the director, and it measures the preferred direction of the rods in the nematic phase.

III. SIMULATION METHOD

We study IN coexistence via grand canonical MC simulations. In the grand canonical ensemble, the volume, the temperature T, and the chemical potential μ are fixed, while the number of rods in the simulation box fluctuates. Insertion and removal of rods are attempted with equal probability and accepted with appropriate Metropolis rules to be given later. The aim of grand canonical simulations is to measure the probability distribution in the number of particles $P(N)$. At the coexistence chemical potential, $P(N)$ becomes bimodal with two peaks of equal area. An example distribution is shown in Fig. 4, where we have plotted the logarithm of $P(N)$. The peak locations yield the coexistence densities; the average height of the peaks $\Delta\Omega$ in $k_{\mathrm{B}}T \ln P(N)$ is the free-energy barrier separating the phases, with k_{B} the Boltzmann constant. In three dimensions using periodic boundary conditions and for sufficiently large systems, the barrier is related to the interfacial tension via $\gamma_{\mathrm{IN}} = \Delta\Omega/(2L_x^2)$, where L_x is the lateral dimension of the simulation box.[23]

In simulations, the free-energy barrier presents a problem. Unless $\Delta\Omega$ is small, such as close to a critical point, simulations rarely cross the barrier, and spend most of the time in only one of the two phases. Biased sampling techniques are required to overcome the barrier. In general, these techniques aim to construct a weight function $W(\zeta)$ of some bias variable ζ. The weight function is constructed such that a simulation using a modified potential $E'(\zeta) = E + k_{\mathrm{B}}TW(\zeta)$ yields a uniform probability distribution in the bias variable, with E the potential of the original system. The grand canonical acceptance rules using the modified potential read as

$$A(N, \zeta_0 \to N+1, \zeta_1) = \min\left[1, \frac{V}{N+1} e^{-\beta(\Delta E - \mu) - W(\zeta_1) + W(\zeta_0)}\right], \tag{4}$$

$$A(N, \zeta_0 \to N-1, \zeta_1) = \min\left[1, \frac{N}{V} e^{-\beta(\Delta E + \mu) - W(\zeta_1) + W(\zeta_0)}\right], \tag{5}$$

for the insertion and removal of a single particle, respectively.[24,25] Here, ζ_0 and ζ_1 denote, respectively, the value of the bias parameter in the initial and final state, ΔE is the potential-energy difference between the initial and final states given by Eq. (2), and $\beta = 1/(k_{\mathrm{B}}T)$. For a properly constructed $W(\zeta)$, the biased simulation samples all states ζ with uniform probability. Once $W(\zeta)$ is known, the distribution $P(N)$ of the unbiased system can be constructed.

One is rather free in choosing the bias variable. The best choices are variables that change significantly when going from one phase to the other. For fluid-vapor transitions, a natural bias is the particle number density. In the case of IN coexistence, the density is still a valid variable because of the density gap between the isotropic and nematic phases. This was used in Ref. 4 to study IN coexistence in suspensions of soft rods. Whether a bias on density in systems of elongated particles is efficient depends on how easily a dense isotropic phase can rearrange itself to become nematic. In practice, the jamming effect limits density-biased sampling to rather small systems and soft interactions. As it turns out, for IN transitions, a much more powerful bias variable is the nematic order parameter S. Note, however, that phase coexistence is defined in terms of $P(N)$. Therefore, in a simulation which biases on S, the distribution $P(N)$ must still be reconstructed. To this end, histograms in both the particle number N, as well as in S, have to be measured. In this section, we explain how the bias on S, and the subsequent reweighting in N and S, are implemented. It is convenient to discuss the more straightforward procedure of a density bias first.

A. Biased sampling on ρ

A convenient method to bias on density is *successive umbrella sampling* (SUS).[26] Here we describe the algorithm in its simplest form; refinements are given in the original reference. The choice of the sampling algorithm is not crucial. The general principles also apply to other schemes, such

as conventional umbrella sampling,[27] multicanonical sampling,[28] Wang-Landau sampling,[29] or hyperparallel tempering.[30]

The aim is to construct a function $W(N)$ of the number of particles such that a simulation using the modified potential $E'(N)=E+k_BTW(N)$ yields a uniform distribution in N, with E given by Eq. (2). The modified potential thus contains an explicit dependence on the bias variable N. Following Ref. 26, the particle number axis is divided into equally sized intervals called windows, starting with some minimum number of particles N_0. In the first window, the number of particles is confined to $N_0 \leqslant N \leqslant N_0+1$, in the second window to $N_0+1 \leqslant N \leqslant N_0+2$, and in the ith window to $N_0+i-1 \leqslant N \leqslant N_0+i$. In this example, the window size equals a single particle, but this choice is not essential: SUS works just as well using larger windows.[26] The choice of the window size is not completely arbitrary. Choosing the windows to be too large leads to poor sampling statistics at the window boundaries; choosing the windows to be too small runs the risk that certain relaxation pathways are cut off. In practice, a compromise needs to be made.

The idea of SUS is to construct $W(N)$ by simulating the windows separately and successively. Starting in the first window ($i=1$), grand canonical MC moves are attempted (optionally combined with canonical moves such as translations and rotations), with the constraint that states that are outside the window bounds are rejected to fulfill detailed balance at the window boundaries. The relevant weights in the first window are $W(N_0)$ and $W(N_0+1)$, which we initially set to zero. We then record f_L^1 and f_H^1, counting the occurrence of the state with N_0 and N_0+1 particles, respectively. In this notation, the subscripts L and H refer to the "lower" and "higher" window bound, respectively, while the superscript refers to the window number. To obtain a uniform distribution in N, the ratio of the counts should be unity. This will generally not be the case, but is enforced by updating the weight of the higher window bound to

$$W_{\text{new}}(N_0+i) = W_{\text{old}}(N_0+i) + \ln(f_H^i/f_L^i), \tag{6}$$

leaving the weight of the lower bound $W(N_0+i-1)$ unchanged, where i is the window number. In case $f_H^i > f_L^i$, the effect of this modification is a lower insertion rate, see Eq. (4), and a higher removal rate, see Eq. (5), leading to a count ratio closer to one. The latter can be checked by performing a second simulation using the updated weight (the reasoning for $f_H^i < f_L^i$ is similar). In practice, it may occur that one of the counts is zero. It is then necessary to modify $W(N_0+i)$ by hand first, before starting the simulation. Note also that long simulation runs may be required to obtain the count ratio accurately.

Having simulated the first window, $W(N_0)$ and $W(N_0+1)$ are known. The choice $W(N_0)=0$ is arbitrary but has no physical consequences, since it merely shifts the potential by a constant. Next, we consider window 2, where the number of particles is allowed to fluctuate between N_0+1 and N_0+2, with respective weights $W(N_0+1)$ and $W(N_0+2)$. An important optimization of Ref. 26 is to linearly extrapolate the known weights $W(N_0)$ and $W(N_0+1)$ to obtain an estimate for $W(N_0+2)$ (note that for the third and subsequent windows, quadratic extrapolation can be used). The simulations in the second window are then performed using the extrapolated estimate, and the respective counts, f_L^2 and f_H^2, of visiting the state with N_0+1 and N_0+2 particles, are recorded. Finally, the weight $W(N_0+2)$ is updated using Eq. (6), leaving the other weight $W(N_0+1)$ unchanged, and the next window is considered.

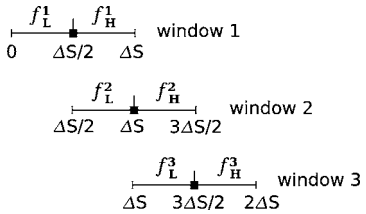

FIG. 1. Schematic illustration of biased sampling on the nematic order parameter. See details in text.

The above procedure is repeated until all windows of interest have been simulated, and the corresponding weight function $W(N)$ is constructed. The sought-for distribution in the number of particles $P(N)$ is trivially obtained via $P(N)=Ce^{W(N)}$, with C a normalization constant.[21]

B. Biased sampling on *S*

Next, we consider the extension to a bias on the nematic order parameter S. Here, the modified potential reads as $E'(S)=E+k_BTW(S)$, with E given by Eq. (2). The aim is to construct $W(S)$ such that a simulation using the modified potential samples all values of S with uniform probability.

The windows are obtained by dividing the nematic order parameter axis into equally sized intervals of width ΔS. In the first window, the nematic order parameter is confined to $0 \leqslant S < \Delta S$, in the second window to $\Delta S/2 \leqslant S < 3\Delta S/2$, and in the ith window to $(i-1)\Delta S/2 \leqslant S < (i+1)\Delta S/2$, see Fig. 1. The windows thus partially overlap. To sample both the isotropic and nematic phases, the sampling range should span from $S=0$ to $S \approx 1$. Note that S is a continuous variable, whereas the density (expressed in the number of particles) is discrete. Therefore, a natural width for the windows does not exist, and one is forced to choose ΔS rather arbitrarily. We found that $\Delta S \approx 0.001-0.002$ gives good results, which means that $\mathcal{O}(10^3)$ windows are required to sample the transition. A consequence of discretizing the nematic order parameter is that $W(S)$ is defined in steps of $\Delta S/2$. Therefore, in the ith window, $W(S)$ assumes only two distinct values

$$W(S) = \begin{cases} W_{i-1}, & (i-1)\Delta S/2 \leqslant S < S_M \\ W_i, & S_M \leqslant S < (i+1)\Delta S/2, \end{cases}$$

with $S_M = i\Delta S/2$ the center of the window (note that $i>0$).

Starting in the first window ($i=1$), the relevant weights are W_0 and W_1, which are initially set to zero. While simulating the first window, we count the occurrence of states with $0 \leqslant S < S_M$ (f_L^1) and $S_M \leqslant S < \Delta S$ (f_H^1), with $S_M = \Delta S/2$. To obtain the distribution in the number of particles $P(N)$ (after all the quantity of interest) particle number histograms must also be stored (note that N fluctuates freely in each window). In the first window, we thus record the probability distribution in the number of particles $p_L^1(N)$ for states with

$0 \leqslant S < S_M$, and $p_H^1(N)$ for states with $S_M \leqslant S < \Delta S$. It is recommended to store the distributions unnormalized. This makes it more convenient to restart the simulations at a later stage in case higher precision is required. After simulating the first window, the weight of the higher window bound is updated to force a uniform distribution in S using $W_{i,\mathrm{new}} = W_{i,\mathrm{old}} + \ln(f_H^i/f_L^i)$, while keeping W_{i-1} fixed, where i is the window number.

In the second window ($i=2$), the relevant weights are W_1 and W_2. To simulate efficiently, the weights W_0 and W_1 of the previous window are extrapolated to estimate W_2. The extrapolated estimate is used while simulating the second window, and the counts f_L^2 and f_H^2 are recorded, as well as the distributions $p_L^2(N)$ and $p_H^2(N)$. After simulating the second window, W_2 is updated as before, and the next window is considered.

The above procedure is repeated up to some maximum number of windows $w_{\max}$ chosen well into the nematic phase. The remaining step is to combine the weights W_i with the distributions $p_L^i(N)$ and $p_H^i(N)$ to obtain $P(N)$. Note that the upper region of window i overlaps with the lower region of the next window $i+1$, see Fig. 1. More precisely, the distributions $p_H^i(N)$ and $p_L^{i+1}(N)$ stem from the same S interval and are thus measured with the same probability by the sampling scheme. Therefore, these distributions may be combined $\bar{p}_i(N) = p_H^i(N) + p_L^{i+1}(N)$, and normalized such that $\sum_{N=0}^{\infty} \bar{p}_i(N) = 1$. The distribution $P(N)$ is simply a weighted sum of the above (normalized) $\bar{p}_i(N)$. Since $-k_B T W_i$ corresponds to a free energy, each $\bar{p}_i(N)$ contributes to $P(N)$ with a weight proportional to e^{W_i}. This leads to $P(N) = C \sum_{i=1}^{w_{\max}} \bar{p}_i(N) e^{W_i}$, where the sum is over all windows, and normalization constant $C^{-1} = \sum_{N=0}^{\infty} \sum_{i=1}^{w_{\max}} \bar{p}_i(N) e^{W_i}$.

C. Bias on ρ versus bias on S

Clearly, the discussed methods serve the same purpose: to measure the distribution $P(N)$ at coexistence. Density-biased sampling is by far the easiest to implement. It has the additional advantage that the coexistence chemical potential need not be specified beforehand: once $P(N)$ has been measured at some chemical potential μ_0, it can be extrapolated to any other chemical potential μ_1 by using the equation

$$P(N|\mu_1) = P(N|\mu_0) e^{\beta(\mu_1 - \mu_0)N}, \tag{7}$$

with $P(N|\mu_\alpha)$ the probability distribution $P(N)$ at chemical potential μ_α. Obviously, one should establish roughly beforehand the density at which the IN transition occurs to avoid sampling large regions of irrelevant phase space.

The situation is reversed when biasing on the nematic order parameter. In this case, the sampling range is always from $S=0$ to $S \approx 1$. However, to observe phase coexistence, it is essential to use a chemical potential that is rather close to the coexistence value. Of course, Eq. (7) still holds, but the range in μ over which one can extrapolate is much smaller, precisely because the bias is put on S and not on ρ. An estimate of the coexistence chemical potential may be obtained in a density-biased simulation of a small system or via the Widom insertion algorithm.[25,31] This certainly makes biasing on S more involved. Moreover, for each attempted MC move, S in the final state must be determined, regardless of whether the move is accepted. It is therefore important to calculate S efficiently. In particular, the $\mathcal{O}(N)$ loop of Eq. (3) should be eliminated, which can be done following the method outlined in Ref. 4.

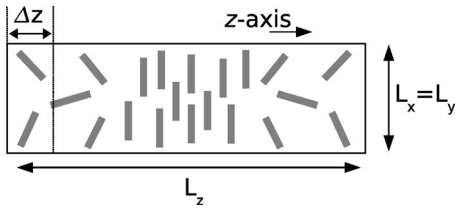

FIG. 2. Schematic representation of a simulation snapshot at IN coexistence. The ordered nematic phase is located in the middle of the simulation box. Profiles are measured along the z dimension using bin-size Δz.

IV. RESULTS

An important conclusion of Ref. 4 is that the IN interfacial tension obtained from $P(N)$ may be prone to strong finite-size effects. Away from any critical point, interfaces are the dominant source of finite size effects. The use of periodic boundary conditions leads to the formation of two interfaces. In small systems, the interfaces may interact and this will influence the estimate of γ_{IN}. A convenient way to suppress interface interactions is to use an elongated simulation box with $L_z \gg L_x$,[32] in accordance with Fig. 2. This forces an orientation of the interfaces perpendicular to the elongated dimension (since this minimizes the interfacial area), with a separation between the interfaces that is larger than it would be in a cubic system of the same volume. The absence of interface interactions is manifested by a pronounced flat region between the peaks in $\ln P(N)$. Note that a flat region is essential, but not sufficient, to extract γ_{IN} reliably. There may still be finite-size effects in the lateral dimensions L_x and L_y, arising for instance from capillary waves. Ideally, the lateral dimensions should be large enough to capture the long-wavelength limiting form of the capillary spectrum.[33] To actually measure the capillary spectrum of the IN interface is demanding.[3] A more convenient approach sufficient for our purposes is to first establish a minimum elongation L_z in which interface interactions are suppressed, and to then check for finite-size effects in the lateral dimensions by varying L_x and L_y explicitly.

An additional motivation to use large lateral dimensions is to stabilize the interfaces. The interfacial free energy is of order $\gamma_{\mathrm{IN}} L_x^2$, and if this is small compared to $k_B T$, the interfaces will generally not be stable. These issues are especially relevant for IN coexistence because γ_{IN} is very small. Therefore, in this section, we first perform MC simulations in the canonical ensemble to obtain an indication of the system size required to observe stable interfaces. Next, we present coexistence data obtained using the nematic order biased-sampling scheme.

A. Interfacial profiles

We consider hard rods, i.e., $\epsilon \to \infty$ in Eq. (1), of elongation $L/D=15$. The simulations are performed in the canoni-

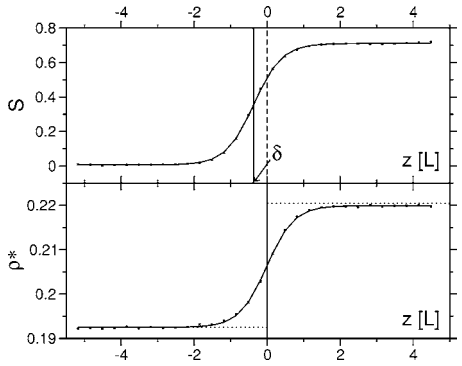

FIG. 3. Nematic order parameter profile $S(z)$ (top), and density profile (bottom) for hard rods with $L/D=15$ across the IN interface. The shift between the profiles is marked δ. Points are raw simulation data; curves are hyperbolic tangent fits. The horizontal lines in the lower frame represent the bulk isotropic and nematic densities obtained in the grand canonical simulations of Sec. IV E.

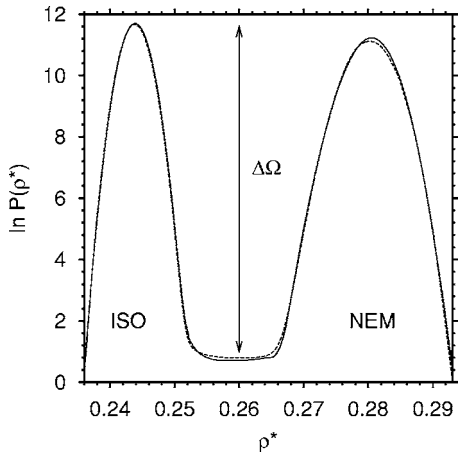

FIG. 4. Coexistence distribution $P(\rho^\star)$ for soft rods with $L/D=15$ and $\beta\epsilon=2$ using box dimensions $L_x=L_y=2.1L$ and $L_z=8.4L$. The solid curve was obtained using a bias on the nematic order parameter S; the dashed curve by using a bias on the density. The average peak height $\Delta\Omega$, multiplied by k_BT, equals the free-energy barrier separating the isotropic (ISO) from the nematic (NEM) phase.

cal ensemble, where the number of rods, the volume, and the temperature are fixed. The box dimensions are $L_x=L_y=10L/3$ and $L_z=20L$. We set the overall density of the system to $\rho^\star=0.205$, which is well inside the coexistence region,[13,14] corresponding to ca. 11 000 particles. An initial system is prepared containing two interfaces, with the director of the nematic phase aligned in the plane of the interface. This is the stable configuration, as confirmed by theory[6,7] and simulation.[2,4,15] The initial system is evolved with random rotations and translations of single rods, accepted with the standard Metropolis rules.[24,25,34] The system is equilibrated for 10^6 sweeps, after which a snapshot is taken every 260 sweeps, up to a total of 3×10^4 snapshots (one sweep corresponds to one attempted MC move per rod).

After equilibration, simulation snapshots schematically resemble Fig. 2. Note, however, that they contain far more particles than depicted in this simple sketch. The aim is to measure the density profile $\rho(z)$, and the nematic order parameter profile $S(z)$ along the elongated z dimension, averaged over many different snapshots. The averages are taken with the center-of-mass of the snapshots shifted to the middle of the simulation box, with the constraint that the nematic phase is also located in the middle, in accordance with Fig. 2. The constraint is necessary to remove ambiguity arising from cases where the isotropic phase is in the middle. Having shifted the center of mass, the density profile is obtained by binning the z axis in steps of $\Delta z\approx0.17L$. The local density $\rho(z)$ in a single snapshot is given by n/υ_B, with n the number of rods in the bin centered around z and υ_B the volume of a single bin. The density profiles are then averaged over all snapshots. Following Ref. 14, for the bin centered around z in a single snapshot, we also define a local orientational tensor $Q(z)$, calculated using Eq. (3) considering only the rods inside the bin. The local orientational tensor elements are then averaged over all snapshots and $S(z)=\mathrm{maxev}\langle Q(z)\rangle$.

The averaged profiles are shown in Fig. 3. The solid curves are hyperbolic tangent fits of the form $A+B\tanh((z-z_c)/w)$, which describe the data well. Note that the profiles are shifted with respect to each other. The magnitude of the shift, measured between the inflection points, equals $\delta=(0.37\pm0.04)L$. This is consistent with theoretical predictions $\delta=(0.45-0.5)L$,[6,35] as well as $\delta\approx0.33L$ obtained in simulations of ellipsoids.[36] Note that the simulated profiles are broadened due to capillary waves.[3] Moreover, we observed considerable fluctuations in the amount of isotropic and nematic phases during the simulation, leading to large fluctuations in the interface positions along the elongated L_z dimension. The width of the averaged profile obtained by fixing the center of mass is therefore additionally broadened.[37,38] Because of these effects, we cannot compare the interfacial width of the simulated profiles to theoretical predictions. More important for our purposes, however, is the observation that the interfaces are stable. For hard rods, the current system size thus seems sufficient to accommodate stable interfaces.

B. Comparison of ρ and S biased sampling

Having established the typical system size required to observe stable interfaces, biased sampling on the nematic order parameter is considered next. First, we show that density- and nematic-order-biased sampling yield the same distribution $P(N)$. To this end, we consider a small system of soft rods with $L/D=15$ and $\beta\epsilon=2$ in a simulation box of size $L_x=L_y=2.1L$ and $L_z=8.4L$. The latter system was investigated in previous work using density-biased sampling.[4] The corresponding coexistence chemical potential reads as $\beta\mu\approx5.15$. The nematic-order-biased sampling scheme is applied to the same system using the latter chemical potential and $\Delta S=0.002$, see Fig. 4. Shown is the coexistence distribution $P(N)$ obtained using a bias on S (solid curve), as well as using a bias on density (dashed curve, reproduced from Ref. 4). The agreement between both methods is strikingly confirmed, thereby justifying the approach of Sec. III B. For small systems, the required CPU time is roughly equal for both methods. The data sets of Fig. 4 required ca. 700 CPU hours each on 2.2-GHz Pentium machines.

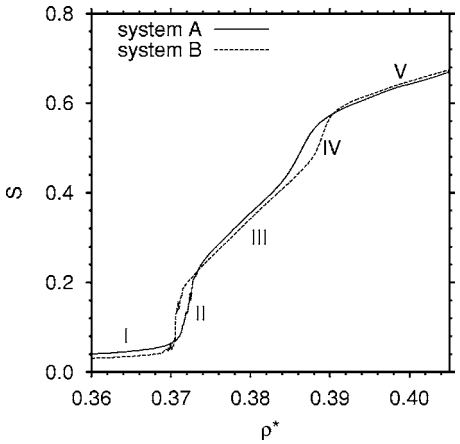

FIG. 5. Dependence of the nematic order parameter on the density for soft rods with $L/D=10$ and $\beta\epsilon=2$, obtained using two different system sizes.

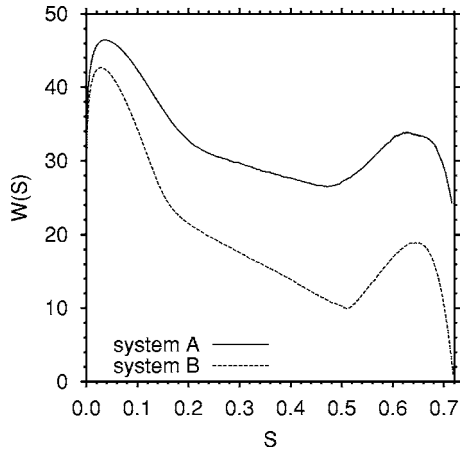

FIG. 6. Weight function $W(S)$ obtained by biasing on the nematic order parameter S (see Sec. III B) for soft rods with $L/D=10$ and $\beta\epsilon=2$ using two different system sizes.

C. Interfacial tension of soft rods

Next, we consider soft rods with $L/D=10$ and $\beta\epsilon=2$. We aim to accurately measure the interfacial tension. To this end, large system sizes are required such that a bias on S is essential. As explained before, the elongated L_z dimension of the simulation box must be large enough to accommodate noninteracting interfaces. At the same time, L_x and L_y must be large enough to suppress finite-size effects in the lateral dimensions. We therefore consider two system sizes: $L_x=L_y=3.5L$, $L_z=10.5L$ (system A) and $L_x=L_y=4L$, $L_z=14L$ (system B), where the lateral dimensions are deliberately chosen to exceed those of Sec. IV A. The simulations are performed using $\Delta S=0.001$ and 0.002, for systems A and B, respectively. An initial estimate of the coexistence chemical potential was taken from previous work.[4]

In Fig. 5, the dependence of the nematic order parameter on the number of particles is shown, calculated using

$$S(N)=C\sum_{i=1}^{w_{\max}} S_i\bar{p}_i(N)e^{W_i}, \tag{8}$$

with $S_i=i\Delta S/2-\Delta S/4$, and the remaining symbols defined as before. Analogous to fluid-vapor transitions,[18,39,40] five distinct regions can be distinguished. In region I, a single isotropic phase is observed. Region II corresponds to the transition from the bulk isotropic phase to the phase with two parallel interfaces. The transition is characterized by the formation of a nematic droplet in an isotropic background, which grows with the density until it self-interacts through the periodic boundaries, ultimately leading to two parallel interfaces. In region III, the interfaces have formed and the system is at coexistence, schematically resembling Fig. 2. Increasing the density further leads to a growth of the nematic domain at the expense of the isotropic domain. Region IV corresponds to the transition to the pure nematic phase, during which the system is characterized by an isotropic droplet in a nematic background. In region V, finally, a single nematic phase is observed.

In Fig. 6, we show the corresponding weight function $W(S)$ for both systems. The double-peaked structure is clearly visible. Note that the isotropic peak is significantly higher than the nematic peak. This indicates that the chemical potential used in the simulations is below the coexistence value. Since coexistence is defined by equal weight in the peaks of $P(N)$, and not in $W(S)$, Fig. 6 cannot be used to obtain the coexistence chemical potential. Instead, $P(N)$ must be constructed first by combining $W(S)$ with the single-window distributions $\bar{p}_i(N)$; Eq. (7) may then be used to extrapolate $P(N)$ to coexistence. The resulting coexistence chemical potential equals $\beta\mu\approx 7.13$ for both systems. In Fig. 7, the logarithm of $P(\rho^\star)$ at coexistence is plotted for both systems, scaled with $L^2/(2L_x^2)$, and the plateaus shifted to zero. In this way, the barrier directly reflects the interfacial tension γ_{IN}, in units of k_BT/L^2.[23] An important observation is that the peaks in both distributions are separated by a pronounced flat region. This shows that the elongated L_z dimension of the simulation box is sufficient. Moreover, the peak heights are similar, indicating that finite-size effects in the lateral dimensions L_x and L_y are also small. Therefore, we conclude that the barrier in Fig. 7 accurately reflects the interfacial tension γ_{IN} for soft rods with $L/D=10$ and $\beta\epsilon=2$. The resulting estimate reads as $\gamma_{\mathrm{IN}}=0.49k_BT/L^2=0.0049k_BT/D^2$.

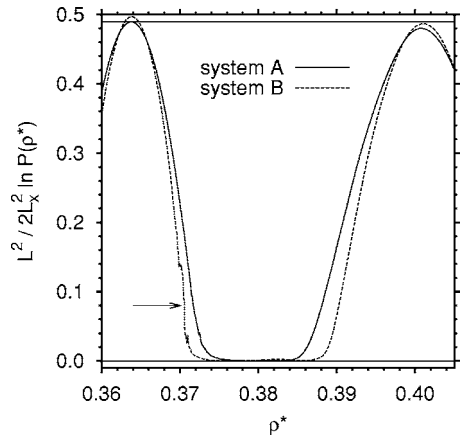

FIG. 7. Logarithm of $P(\rho^\star)$ at coexistence for soft rods with $L/D=10$ and $\beta\epsilon=2$ using two different system sizes. Note the flat region in between the peaks. The arrow indicates transition II of Fig. 5.

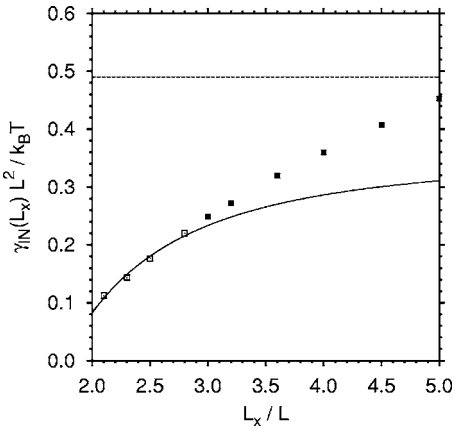

FIG. 8. Interfacial tension $\gamma_{IN}(L_x)$ obtained in cubic systems with edge L_x, as function of L_x, for soft rods with $L/D=10$ and $\beta\epsilon=2$.

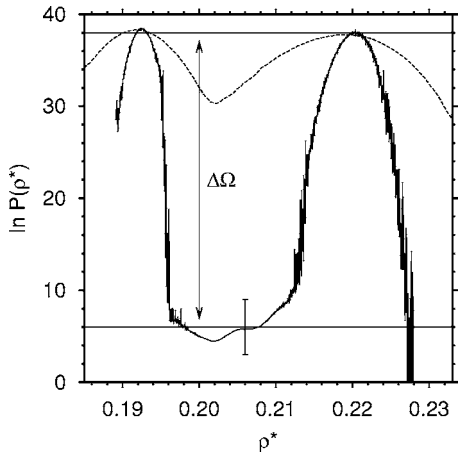

FIG. 9. Coexistence distribution (solid curve) for hard rods with $L/D=15$, obtained using box dimensions $L_x=L_y=10L/3$ and $L_z=10L$. The barrier $\Delta\Omega$ is measured between the horizontal lines, where the bar gives an indication of the uncertainty. The dashed curve shows $P(\rho^\star)$ obtained in a smaller cubic box with $L_x=2.3L$.

In the nematic phase, ca. 6000 rods were simulated for system A and 10 000 for system B. To obtain reliable results, a substantial investment in CPU time is thus required (ca. 3200 CPU hours were invested for system B). Since biased sampling schemes are easy to parallelize, results can typically be obtained within 1–2 weeks on a modern computer cluster. Accurate sampling is especially important around transitions II and IV, and this becomes increasingly difficult in large systems.[40] This may already be inferred from the scatter in the data of system B around transition II (arrow in Fig. 7). Transition IV, on the other hand, is sampled with surprisingly little difficulty. The likely explanation is that process II requires the formation of a nematic nucleus, whose director is aligned in the *xy* plane. Process IV, on the other hand, does not require any preferred orientation of the (isotropic) nucleus, and is therefore easier to sample.

D. Consequences for finite-size extrapolation

An alternative method to obtain the interfacial tension is to measure $\gamma_{IN}(L_x)$ in cubic systems with edge L_x, and use the extrapolation equation of Binder,[23]

$$\gamma_{IN}(L_x) = \gamma_{IN} + a/L_x^2 + b\,\ln(L_x)/L_x^2, \tag{9}$$

to estimate γ_{IN}. In principle, this approach enables estimates of γ_{IN} through an elimination of finite- size effects, but it requires estimates over a range of values for which $\gamma_{IN}(L_x)L_x^2/k_BT \gg 1$. In practice, however, one often tries to use Eq. (9) using data from smaller systems. In Ref. 4, this approach was applied to soft rods with $L/D=10$ and $\beta\epsilon=2$, assuming $b=0$ in Eq. (9), leading to $\gamma_{IN}=0.0035k_BT/D^2$. This estimate differs profoundly from the one of the previous section, implying that finite-size extrapolation must be used with care. The issue is investigated further in Fig. 8. Shown is $\gamma_{IN}(L_x)$ as a function of L_x, where the open squares are data from Ref. 4 and closed squares are data from larger systems obtained in this work. The horizontal line corresponds to the estimate of Fig. 7. Note that the data indeed approach the latter estimate. The curve is a fit to the open squares using Eq. (9) with $b=0$, which summarizes the result of Ref. 4. Clearly, the fit fails to capture the data of the larger systems. Allowing b in Eq. (9) to be nonzero will obviously lead to a better fit, but the resulting γ_{IN} depends sensitively on the range over which the fit is performed, making this approach somewhat arbitrary. The problem partly stems from the difficulty in distinguishing a/L_x^2 numerically from $b\,\ln(L_x)/L_x^2$, since the range in L_x that can be sampled is rather small. Additionally, in small systems, the interface interactions may be strong. This will introduce corrections to Eq. (9), which may even yield nonmonotonic behavior in $\gamma_{IN}(L_x)$.[41–43] As a result, it is difficult to extract γ_{IN} via finite-size extrapolation. In contrast, by using an elongated simulation box, and by explicitly checking for finite-size effects in the lateral dimensions, γ_{IN} can be extracted reliably as shown in Fig. 7. This, we conclude in hindsight, should be the method of choice.

E. Interfacial tension of hard rods

Finally, we apply nematic-order-biased sampling to a system of hard rods with $L/D=15$, system size $L_x=L_y=10L/3$, and $L_z=10L$, corresponding to ca. 6000 rods in the nematic phase. An initial estimate of the coexistence chemical potential was obtained via Widom insertion.[31] The nematic order parameter is sampled with resolution $\Delta S=0.0025$ to obtain $W(S)$. Combining $W(S)$ with the single window distributions $\bar{p}_i(N)$ and applying Eq. (7) yields for the coexistence chemical potential $\beta\mu \approx 5.58$. The corresponding coexistence distribution is shown in Fig. 9.

Note that $P(N)$ for hard rods is prone to substantial statistical error. This is to be expected because the acceptance rate of grand canonical insertion for hard rods is only 0.004%, compared to 8% for soft rods. Nevertheless, the double-peaked structure is clearly visible. From the average peak locations, we obtain $\rho^\star_{ISO}=0.193$ and $\rho^\star_{NEM}=0.220$. The latter densities are consistent with the bulk plateaus in the density profile, indicated by the horizontal lines in Fig. 3. To further check the consistency of our results, an additional simulation in a smaller cubic system with $L_x=2.3L$ was performed; the corresponding coexistence distribution is shown dashed in Fig. 9. Of course, this system is too small to ex-

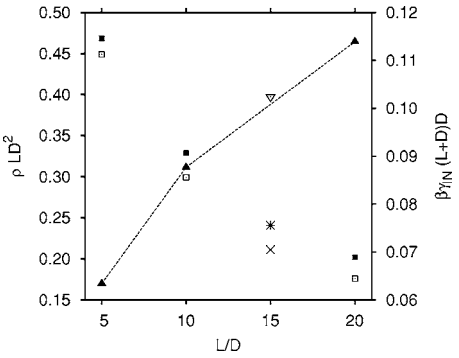

FIG. 10. IN coexistence properties of the hard-rod fluid obtained by theory (Ref. 9), compared to simulation results obtained in this work. The symbols are explained in the text.

tract the interfacial tension, but the peak positions, and hence the coexistence densities, agree well with those of the larger system. The agreement with bulk densities obtained via Gibbs ensemble simulations[14] and Gibbs-Duhem integration[13] is better than 4%. The height of the free-energy barrier of the larger system reads as $\Delta\Omega=(32\pm3)k_BT$, leading to an interfacial tension $\gamma_{IN}\approx1.4k_BT/L^2=0.0064k_BT/D^2=0.096k_BT/LD=0.10k_BT/(L+D)D$.

V. DISCUSSION AND SUMMARY

In this paper, we have presented methodic developments that allow for the estimation of the interfacial tension between isotropic and nematic phases in suspensions of rods. The problem is challenging because γ_{IN} is very small, and methods that work well for interfaces between isotropic phases become problematic, such as exploiting the anisotropy of the pressure tensor,[33] or analyzing the capillary wave spectrum (the latter requires very precise data from huge systems[3]). The novelty of the present approach is to combine grand canonical MC simulations with a bias on the nematic order parameter and obtain γ_{IN} from the grand canonical distribution $P(N)$. The advantage is that the problem of "jamming" is largely solved, enabling simulations of large systems.

The current approach also allows for grand canonical simulations of hard rods, enabling a direct comparison to theory. In the Onsager limit of infinite rod length, theoretical estimates of γ_{IN} typically range from 0.156 (Ref. 11) to 0.34,[44] in units of k_BT/LD. As expected, this exceeds the value for hard rods obtained in this work ($\gamma_{IN}\approx0.096k_BT/LD$) because $L/D=15$ is still far from the Onsager limit. As shown by experiment[1] and theory,[9] γ_{IN} increases with L/D. The latter theory is based on the Somoza-Tarazona density functional[45] and its main findings are summarized in Fig. 10. Shown are the coexistence densities (left axis) and the interfacial tension (right axis) as functions of the rod elongation L/D, where we have adopted the units of Ref. 9. Open and closed squares show the theoretical density of the isotropic and nematic phases, respectively; the star and the cross are the corresponding simulation estimates of this work. The closed triangles are the theoretical interfacial tension, where the line serves to guide the eye; the open triangle represents the simulation estimate of γ_{IN}. Theoretical estimates are reported for $L/D=5,10,20$, but unfortunately not for $L/D=15$. This makes a direct comparison difficult; interpolation of the theoretical results, however, seems in good agreement with our simulation results, as may be inferred from Fig. 10.

A typical rod dimension in experiments is $L=150$ nm and $\gamma_{IN}=0.000\,83$ mN/m.[1] For $T=298$ K, this length translates into 0.000 25 mN/m using our estimate of γ_{IN}. Obviously, this estimate differs from the experimental one because the hard-rod fluid is a simplified model, but it is reassuring to see that the order of magnitude is confirmed.

The current biased-sampling scheme thus seems well suited to simulate IN coexistence, even for hard interactions. Our scheme may also be useful for the application of transition path sampling[46] to anisotropic colloidal systems, since it can provide valuable starting paths; work along these lines is in progress. The remaining bottleneck is the low acceptance rate of grand canonical insertion. It remains a challenge to address this final problem. Since the overall density around the IN transition is low, it is anticipated that higher acceptance rates can be realized using smarter insertion schemes. To develop such schemes would be the subject of future work.

ACKNOWLEDGMENTS

We thank the Deutsche Forschungsgemeinschaft (DFG) for support (TR6/A5 and TR6/D5) and K. Binder, M. Müller, P. Virnau, P. van der Schoot, R. van Roij, and M. Dijkstra for a careful reading of the manuscript and/or helpful suggestions. One of the authors (T.S.) is supported by the Emmy Noether program of the DFG. Allocation of computer time on the JUMP at the Forschungszentrum Jülich is gratefully acknowledged. T. S. also acknowledges financial support by the MWFZ of Rheinland Pfalz.

[1] W. Chen and D. G. Gray, Langmuir **18**, 663 (2002).
[2] A. J. McDonald, M. P. Allen, and F. Schmid, Phys. Rev. E **63**, 010701(R) (2000).
[3] N. Akino, F. Schmid, and M. P. Allen, Phys. Rev. E **63**, 041706 (2001).
[4] R. L. C. Vink and T. Schilling, Phys. Rev. E **71**, 051716 (2005).
[5] D. J. Cleaver and M. P. Allen, Mol. Phys. **80**, 253 (1993).
[6] Z. Y. Chen and J. Noolandi, Phys. Rev. A **45**, 2389 (1992).
[7] D. L. Koch and O. G. Harlen, Macromolecules **32**, 219 (1999).
[8] P. van der Schoot, J. Phys. Chem. B **103**, 8804 (1999).
[9] E. Velasco, L. Mederos, and D. E. Sullivan, Phys. Rev. E **66**, 021708 (2002).
[10] M. P. Allen, Chem. Phys. Lett. **331**, 513 (2000).
[11] K. Shundyak and R. van Roij, J. Phys.: Condens. Matter **13**, 4789 (2001).
[12] L. Onsager, Ann. N.Y. Acad. Sci. **51**, 627 (1949).
[13] P. Bolhuis and D. Frenkel, J. Chem. Phys. **106**, 666 (1997).
[14] M. Dijkstra, R. van Roij, and R. Evans, Phys. Rev. E **63**, 051703 (2001).
[15] M. S. Al-Barwani and M. P. Allen, Phys. Rev. E **62**, 6706 (2000).
[16] J. Potoff and A. Panagiotopoulos, J. Chem. Phys. **112**, 6411 (2000).
[17] W. Góźdź, J. Chem. Phys. **119**, 3309 (2003).
[18] P. Virnau, M. Müller, L. G. MacDowell, and K. Binder, J. Chem. Phys. **121**, 2169 (2004).
[19] M. Müller and L. G. MacDowell, Macromolecules **33**, 3902 (2000).
[20] R. L. C. Vink and J. Horbach, J. Chem. Phys. **121**, 3253 (2004).
[21] N. B. Wilding, Am. J. Phys. **69**, 1147 (2001).
[22] S. R. Williams and A. P. Philipse, Phys. Rev. E **67**, 051301 (2003).
[23] K. Binder, Phys. Rev. A **25**, 1699 (1982).
[24] D. P. Landau and K. Binder, *A Guide to Monte Carlo Simulations in Statistical Physics* (Cambridge University Press, Cambridge, 2000).

[25] D. Frenkel and B. Smit, *Understanding Molecular Simulation* (Academic, San Diego, 2001).
[26] P. Virnau and M. Müller, J. Chem. Phys. **120**, 10925 (2004).
[27] G. M. Torrie and J. P. Valleau, J. Comput. Phys. **23**, 187 (1977).
[28] B. Berg and T. Neuhaus, Phys. Rev. Lett. **68**, 9 (1992).
[29] F. Wang and D. P. Landau, Phys. Rev. Lett. **86**, 2050 (2001).
[30] Q. Yan and J. J. de Pablo, J. Chem. Phys. **113**, 1276 (2000).
[31] B. Widom, J. Chem. Phys. **39**, 2802 (1963).
[32] B. Grossmann and M. L. Laursen, Nucl. Phys. B **408**, 637 (1993).
[33] J. S. Rowlinson and B. Widom, *Molecular Theory of Capillarity* (Clarendon, Oxford, 1982).
[34] M. E. J. Newman and G. T. Barkema, *Monte Carlo Methods in Statistical Physics* (Clarendon, Oxford, 1999).
[35] K. Shundyak and R. van Roij, Phys. Rev. E **68**, 061703 (2003).
[36] M. P. Allen, J. Chem. Phys. **112**, 5447 (2000b).
[37] K. Binder and M. Müller, Int. J. Mod. Phys. C **11**, 1093 (2000).
[38] H. L. Tepper and W. J. Briels, J. Chem. Phys. **116**, 5186 (2002).
[39] P. Virnau, L. G. MacDowell, M. Müller, and K. Binder, in *High Performance Computing in Science and Engineering*, edited by S. Wagner, W. Hanke, A. Bode, and F. Durst (Springer, Berlin, 2004), p. 125.
[40] L. G. MacDowell, P. Virnau, M. Müller, and K. Binder, J. Chem. Phys. **120**, 5293 (2004).
[41] K. K. Mon, Phys. Rev. Lett. **60**, 2749 (1988).
[42] B. A. Berg, U. Hansmann, and T. Neuhaus, Z. Phys. B: Condens. Matter **90**, 229 (1993).
[43] J. E. Hunter III and W. P. Reinhardt, J. Chem. Phys. **103**, 8627 (1995).
[44] W. E. McMullen, Phys. Rev. A **38**, 6384 (1988).
[45] A. M. Somoza and P. Tarazona, J. Chem. Phys. **91**, 517 (1989).
[46] P. G. Bolhuis, D. Chandler, C. Dellago, and P. L. Geissler, Annu. Rev. Phys. Chem. **53**, 291 (2002).